Electronic Supplementary Material (ESI) for Catalysis Science & Technology.

Copper nanoparticles decorated polyaniline-zeolite nanocomposite for the nanomolar simultaneous detection of hydrazine and phenylhydrazine

Balwinder Kaur, Rajendra Srivastava*, and Biswarup Satpati

Supporting Information

Chronoamperometry study

Chronoamperometry was used to calculate the diffusion coefficient (D) and rate constant (k) for the electro-catalytic reaction (Fig. S6-S7). Chronoamperograms were obtained at different concentrations of analytes at a desired potential step (450 and 650 mV for PhZ and HZ, respectively) (Fig. S6-S7). The plots of I verses $t^{-1/2}$ exhibited straight lines for different concentrations of analytes (Fig. S6-S7, inset a). Cottrell equation (Eq. 1) was used to calculate the diffusion coefficient for various analytes investigated in this study.[1]

$$I_p = n\,F\,A\,D^{1/2}\,c/\pi^{1/2}\,t^{1/2} \qquad (1)$$

Where I_p is the catalytic current of CuNPs(5%)-PANI-Nano-ZSM-5/GCE in the presence of analyte, F is the Faraday constant (96485 C/mole), A is the geometric surface area of the electrode (0.07 cm^2), D is the diffusion coefficient (cm^2/s), c is the analyte concentration (mol/cm^3), and t is the time elapsed (s). The diffusion coefficients were found to be 8.4×10^{-6} and 34.8×10^{-6} cm^2/s for HZ and PhZ, respectively.

Chronoamperometry was also employed to calculate the rate constant (k) for electro-catalytic reaction through Eq. 2. [2]

$$I_C/I_L = \gamma^{1/2}\,[\pi^{1/2}\,\mathrm{erf}\,(\gamma^{1/2}) + \exp\,(-\gamma)/\gamma^{1/2}] \qquad (2)$$

Where I_C is the catalytic current of CuNPs(5%)-PANI-Nano-ZSM-5/GCE in the presence of analyte, I_L is the limiting current in the absence of analyte and = kC_0t (C_0 is the bulk concentration of analyte) is the argument of the error function. In cases, where e xceed 2, the error function is almost equal to 1 and the above equation can be reduced to:

$$I_C/I_L = \pi^{1/2}\,\gamma^{1/2} = \pi^{1/2}\,(kC_0t)^{1/2} \qquad (3)$$

Where k, C_0 and t are the catalytic rate constant (1/M s), analyte concentration (M), and time elapsed (s), respectively. Eq. 3 can be used to calculate the rate constant of the catalytic process. Based on the slope of I_C/I_L vs. $t^{1/2}$ plot; k can be obtained for a given analyte concentration (Fig. S6-S7, inset b). From the values of the slopes, an average value for k was obtained for the

oxidation of analyte. The rate constant values for electro-catalytic oxidation of HZ and PhZ were found as 9.8×10^4 and 1.1×10^4 1/s M, respectively.

FT-IR investigation of synthesized materials

Figure S1 shows the FT-IR spectrum of PANI, Nano-ZSM-5, and PANI-Nano-ZSM-5 samples. FT-IR absorption peaks at 1578 and 1497 cm^{-1} in PANI sample are due to C=C stretching of quinoid and benzenoid ring in PANI.[3, 4] The bands at 1300 and 825 cm^{-1} can be assigned to N–H bending mode and out of plane deformation of C–H (benzene ring) in the PANI sample. The strong peak at 1128 cm^{-1} is due to the degree of electron delocalization in PANI and stretching of N=Q=N in quinoid (Q) ring.[5] The characteristic band at 1236 cm^{-1} can be assigned to $C\text{-}N^{\bullet+}$ stretching vibration in PANI. The peaks at 1387 cm^{-1} can be assigned to the stretching vibrations of secondary aromatic C-N. Peaks at 1050 and 700 cm^{-1} (due to S=O and S-O) confirm the incorporation of sulfonate groups attached to the aromatic rings in PANI structure. Nano-ZSM-5 exhibited several common IR peaks at 800 cm^{-1}, 970 cm^{-1}, 1100 cm^{-1}, and 1230 cm^{-1} (Figure S1).[6] The absorption peak at 800 cm^{-1} is due to Si−O−Si symmetric stretching. The absorption peaks at 1100 cm^{-1} and 1230 cm^{-1} are assigned to asymmetric stretching of Si−O−Si whereas peak at 970 cm^{-1} is due to the incorporation of Al in the MFI framework and assigned to an asymmetric stretching mode of a $[SiO_4]$ unit bonded to a M^{4+} ion (O_3Si–O–M). Nano-ZSM-5-Pr-NH_2 exhibited IR peaks at 2930 and 2842 cm^{-1}, which are characteristics of asymmetric and symmetric –CH_2 stretching vibrations in the propyl chain, respectively.[7] The absorption bands at 1596 and 1410 cm^{-1} are assigned to the bending mode of the -NH_2 group and to the scissor vibration of -NH, respectively. The absorption band at 1470 cm^{-1} is due to –CH_2 bending (scissoring) vibration. The C-N stretching frequency for the aminopropyl moiety is observed at 1189 cm^{-1}. A strong peak at 800 cm^{-1} represents the Si-O-Si bond symmetrical stretching vibration.[7] These observations confirmed the incorporation of propylamine moiety on the surface of Nano-ZSM-5. The FT-IR spectrum for PANI-Nano-ZSM-5 exhibited the IR peaks corresponding to both Nano-ZSM-5 and PANI phases which confirms the presence of both phases in the PANI-Nano-ZSM-5 nanocomposite material.

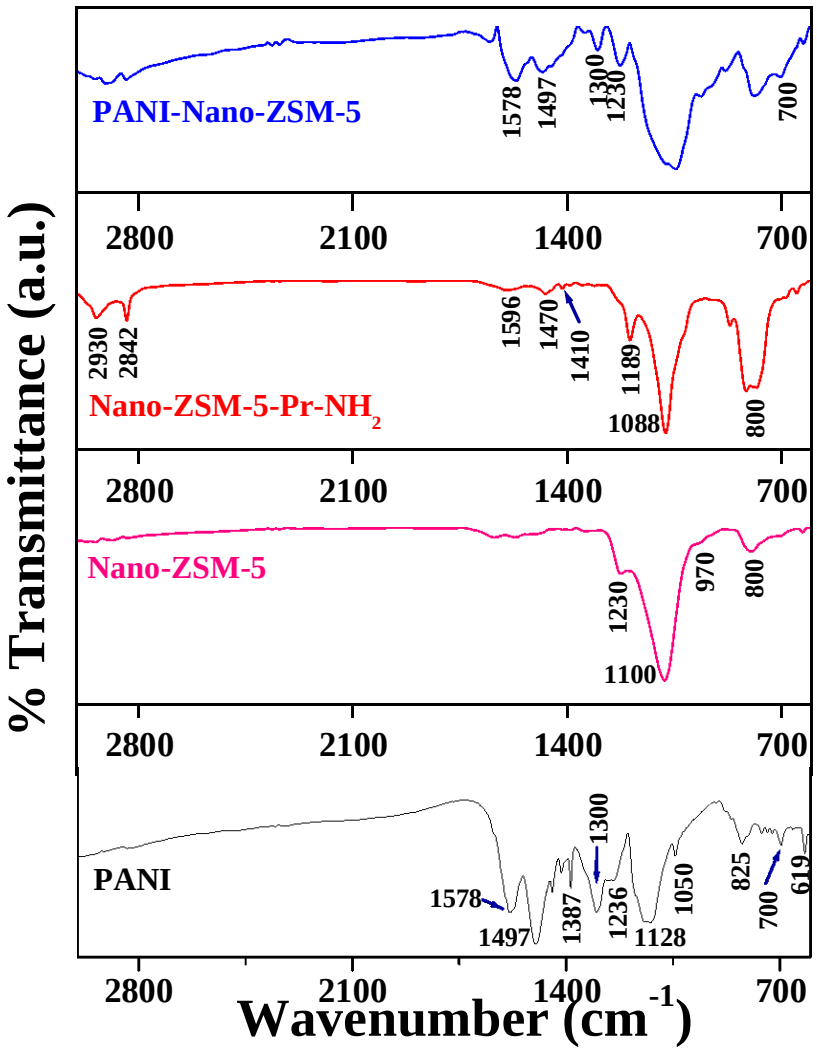

Figure S1. FT-IR spectrum of different PANI/Nano-ZSM-5 materials investigated in the study.

TGA investigation of synthesized materials

Figure S2 shows the TGA curves for PANI-Nano-ZSM-5, Nano-ZSM-5-Pr-NH_2, Nano-ZSM-5, and conventional PANI. The first weight loss below 473 K in the TGA curves for all the samples indicates the loss of physically adsorbed water molecules. The TGA curve for Nano-ZSM-5 showed no appreciable weight loss after 473 K, confirming that chemical composition did not change in this temperature range. In the TGA curve for conventional PANI, the second sharp weight loss between 533-603 K may be attributed to the evaporation or decomposition of few unstable oligoanilines/dopants and the third weight loss after 603 K is attributed to the decomposition of PANI polymer chains. The total weight loss of PANI was 100 % and combustion of PANI in air stream was completed at 913 K. In the TGA curve for Nano-ZSM-5-Pr-NH_2, the second weight loss between 525-875 K can be attributed to the decomposition of organic propylamine moiety anchored on the surface of Nano-ZSM-5 and the residual weight refers to the content of Nano-ZSM-5 in Nano-ZSM-5-Pr-NH_2. TGA analysis confirmed that Nano-ZSM-5-Pr-NH_2 contains 11 wt % functionalized organic group (-Pr-NH_2). In the TGA curve for PANI-Nano-ZSM-5, the combustion of PANI in air stream was completed at 913 K and the residual weight refers to the content of Nano-ZSM-5 in the nanocomposite. TGA confirms that PANI-Nano-ZSM-5 nanocomposite contains 40.7 wt % Nano-ZSM-5 and 43.8 wt % PANI. Nano-ZSM-5/PANI weight ratio was found to be 0.93, which was very close to their initial weight ratio.

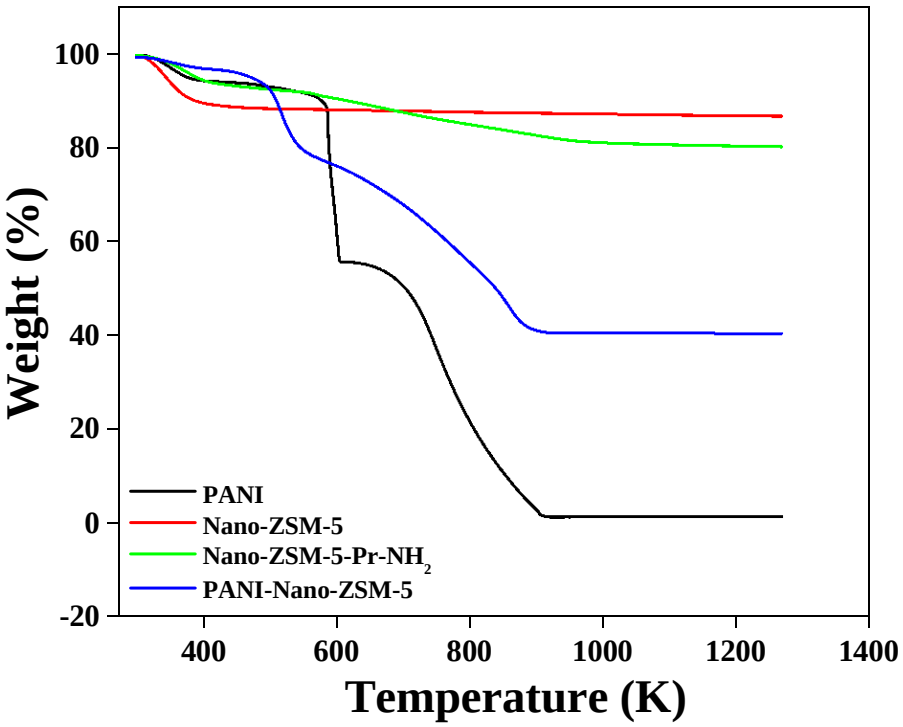

Figure S2. TGA thermograms of PANI, Nano-ZSM-5, PANI-Nano-ZSM-5-Pr-NH_2, and PANI-Nano-ZSM-5 materials at a heating rate of 10 K/min recorded in air stream.

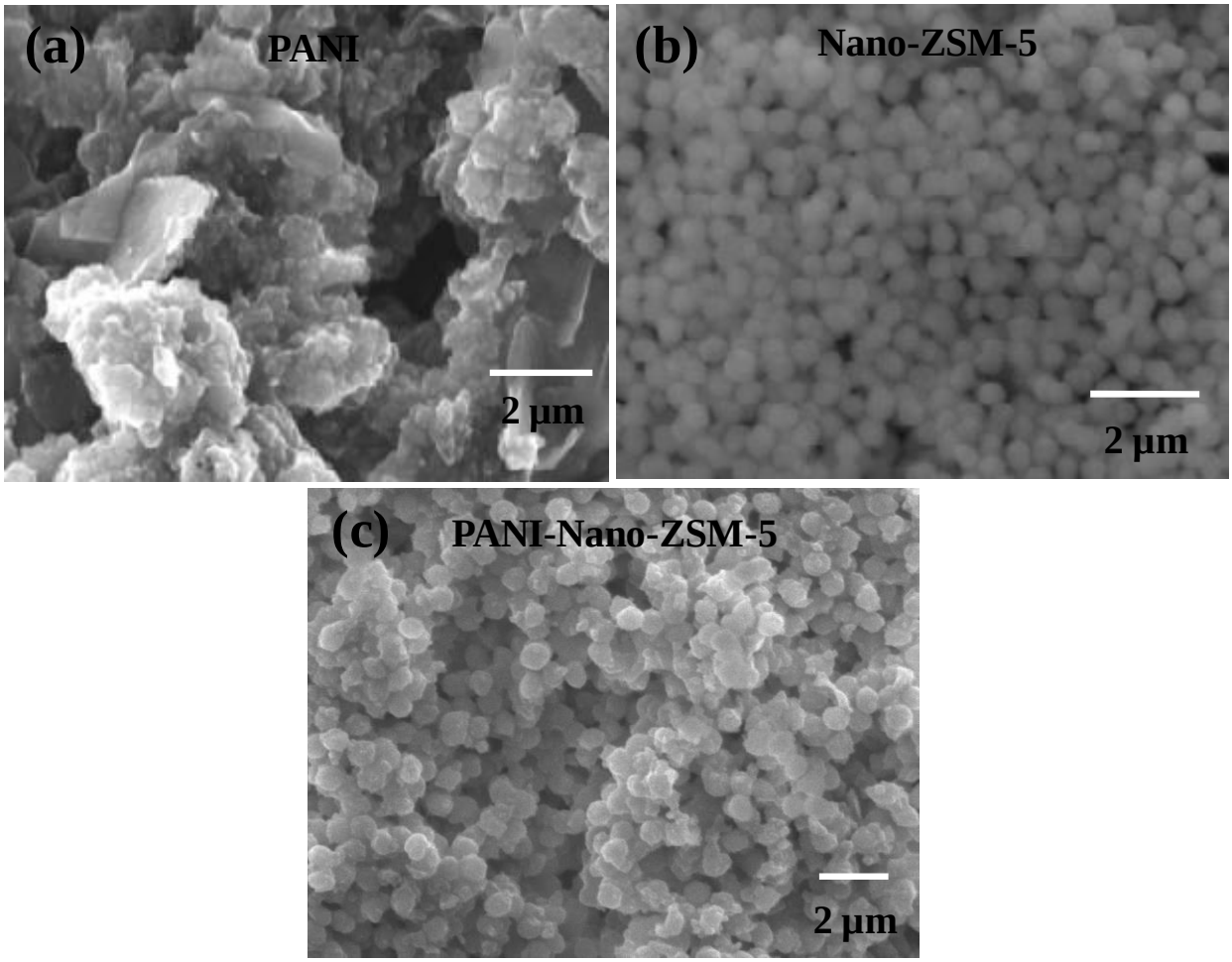

Figure S3. SEM images for PANI, Nano-ZSM-5, and PANI-Nano-ZSM-5 materials.

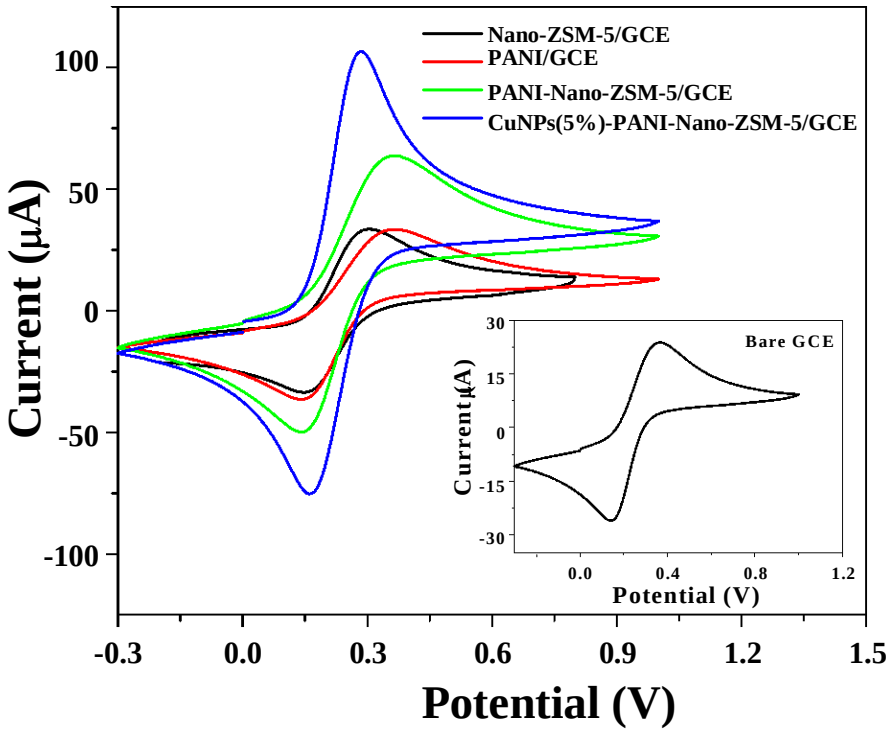

Figure S4. CV responses of various modified electrodes (CuNPs(5%)-PANI-Nano-ZSM-5/GCE, PANI-Nano-ZSM-5/GCE, PANI/GCE, Nano-ZSM-5/GCE) and bare GCE (Inset) in 0.1 M KCl solution containing 1 mM of $[Fe(CN)_6]^{3-/4-}$ at a scan rate of 10 mV/s.

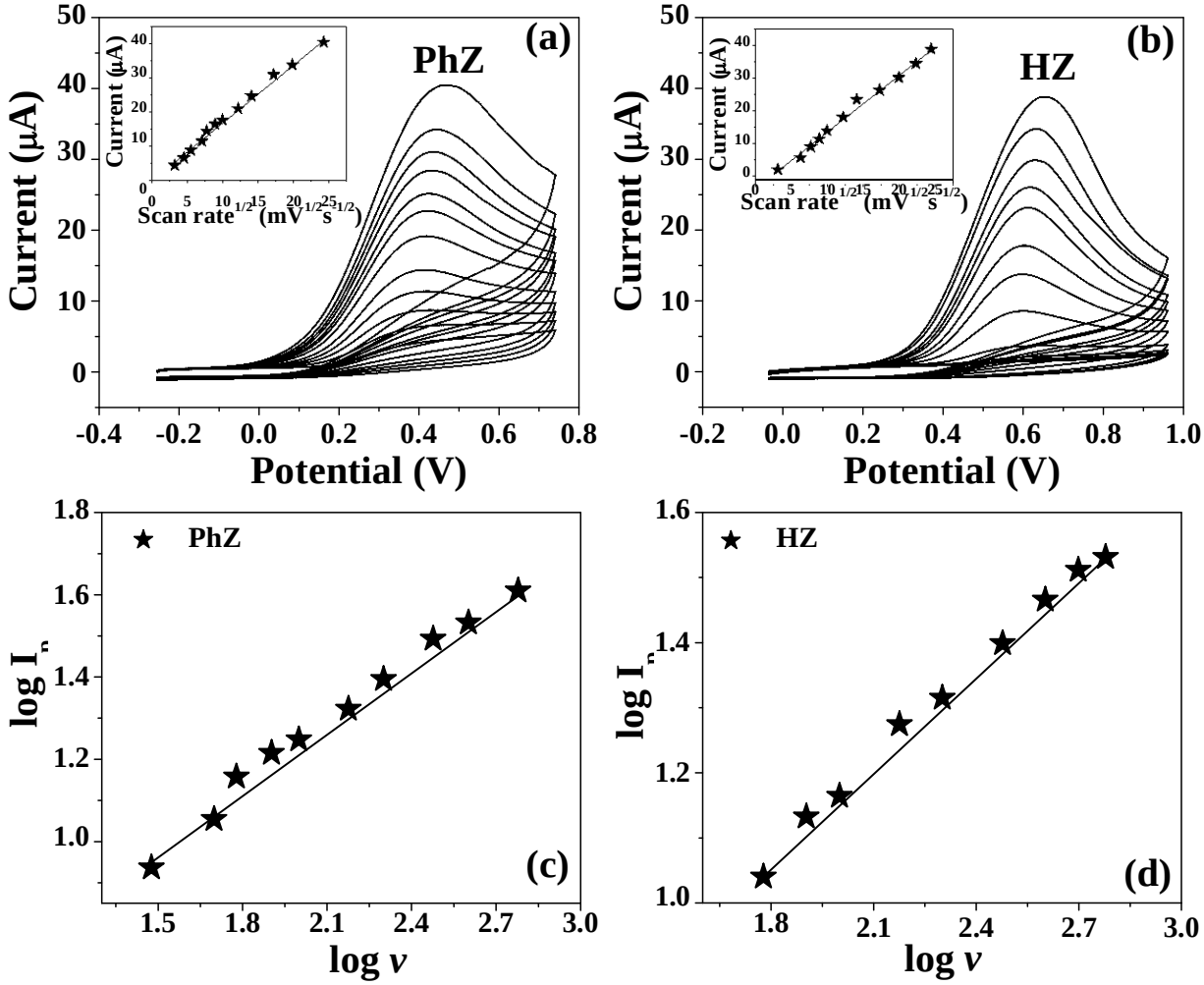

Figure S5. CVs at CuNPs(5%)-PANI-Nano-ZSM-5/GCE containing (a) PhZ (10 µM), (b) HZ (10 µM) in 0.1 M PBS (pH 8.5) at various scan rates (10-600 mV/s). Inset shows the plot of oxidation peak currents vs. square root of scan rates. (c)-(d) Plot of log I_p and log scan rate (ν) for the electrochemical oxidation of (c) PhZ, and (d) HZ at CuNPs(5%)-PANI-Nano-ZSM-5/GCE.

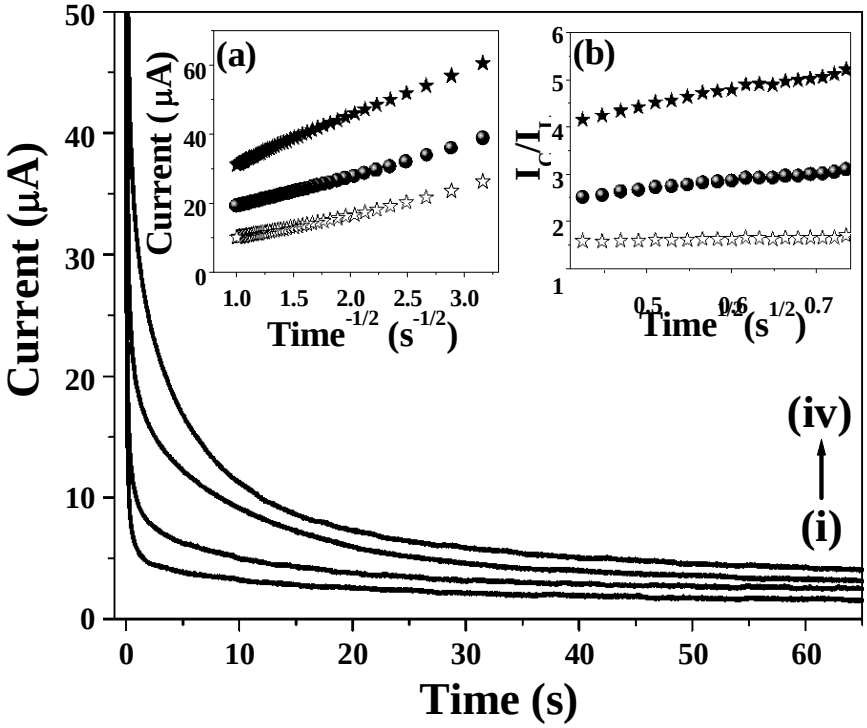

Figure S6. Chronoamperograms obtained at CuNPs(5%)-PANI-Nano-ZSM-5/GCE (i) in the absence and in the presence of (ii) 100 µM, (iii) 200 µM, and (iv) 300 µM of PhZ in 10 mL 0.1 M PBS (pH 8.5). Inset: (a) Dependence of current on the time$^{-1/2}$ derived from the chronoamperogram data. (b) Dependence of I_C/I_L on time$^{1/2}$ derived from the data of chronoamperograms.

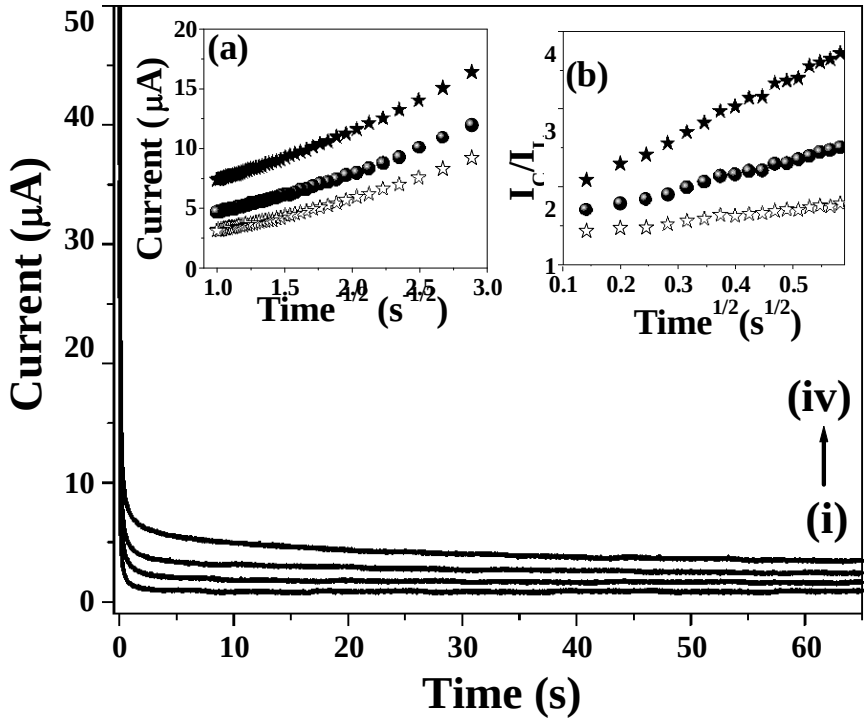

Figure S7. Chronoamperograms obtained at CuNPs(5%)-PANI-Nano-ZSM-5/GCE (i) in the absence and in the presence of (ii) 100 µM, (iii) 200 µM, and (iv) 300 µM of HZ in 10 mL 0.1 M PBS (pH 8.5). Inset: (a) Dependence of current on the time$^{-1/2}$ derived from the chronoamperogram data. (b) Dependence of I_C/I_L on time$^{1/2}$ derived from the data of chronoamperograms.

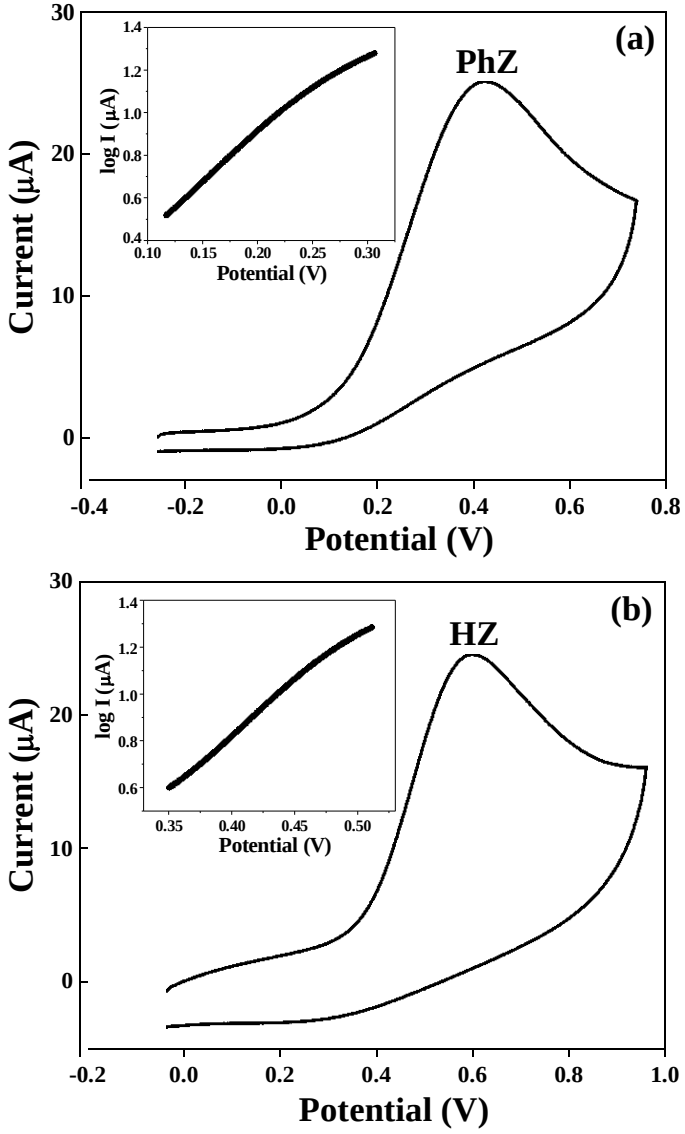

Figure S8. CVs of CuNPs(5%)-PANI-Nano-ZSM-5/GCE in the presence of 10 µM (a) PhZ and (b) HZ in 0.1 M PBS (pH 8.5) at a scan rate of 50 mV/s. Inset shows the tafel plot of CV of 10 µM (a) PhZ and (b) HZ at a scan rate of 50 mV/s.

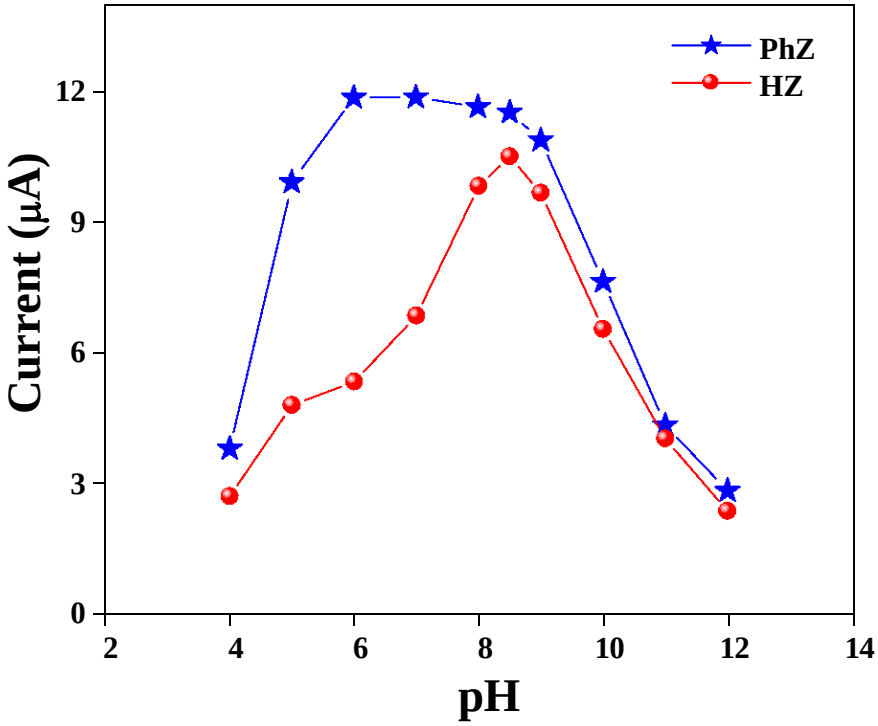

Figure S9. Influence of the pH on the oxidation peak currents of PhZ and HZ at CuNPs(5%)-PANI-Nano-ZSM-5/GCE.

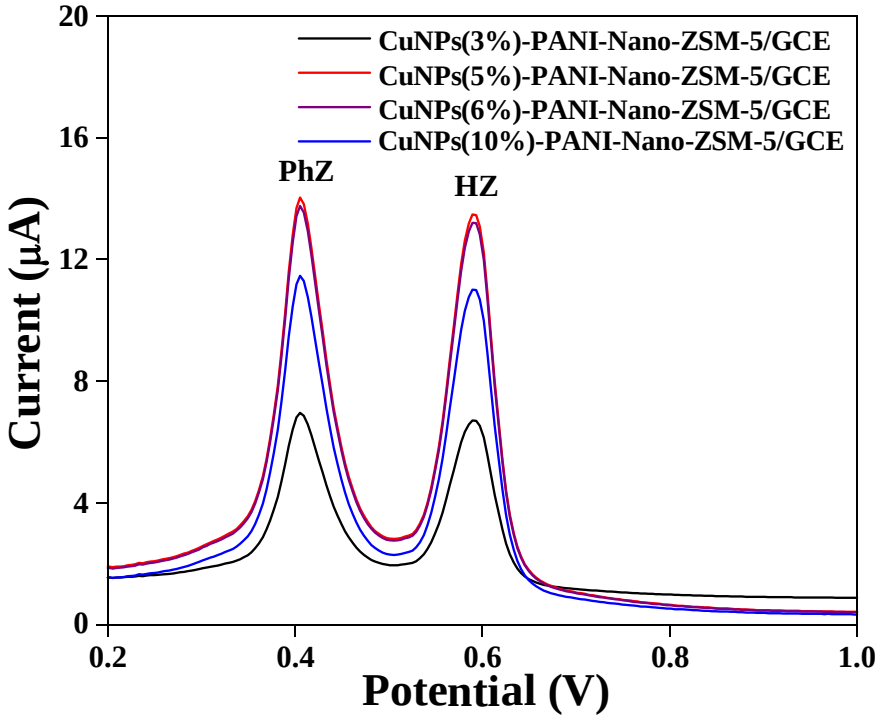

Figure S10. DPVs in the presence of 5 µM each of PhZ and HZ in 10 mL of 0.1 M PBS (pH 8.5) at CuNPs(3%)-PANI-Nano-ZSM-5/GCE, CuNPs(5%)-PANI-Nano-ZSM-5/GCE, CuNPs(6%)-PANI-Nano-ZSM-5/GCE, and CuNPs(10%)-PANI-Nano-ZSM-5/GCE. DPV parameters were selected as: pulse amplitude: 50 mV, pulse width: 50 ms, scan rate: 20 mV/s.

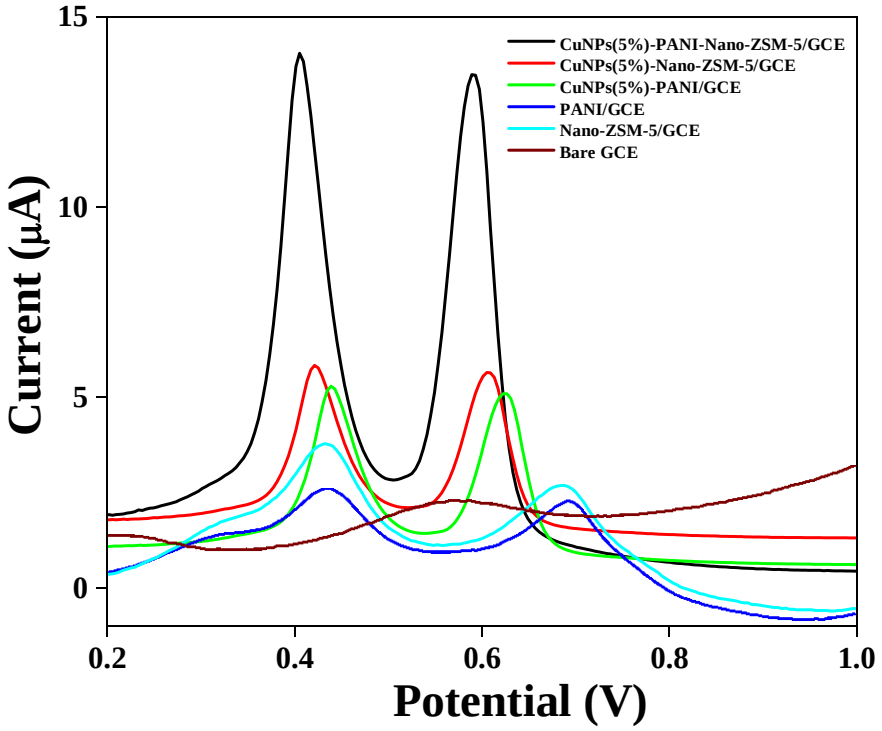

Figure S11. Comparison of DPV of binary mixture containing 5 μM each of PhZ and HZ at various modified electrodes (Cu(5%)-PANI-Nano-ZSM-5/GCE, Cu(5%)-Nano-ZSM-5/GCE, Cu(5%)-PANI/GCE, PANI/GCE, Nano-ZSM-5/GCE) and bare GCE in 0.1 M PBS (pH 8.5). DPV parameters were selected as: pulse amplitude: 50 mV, pulse width: 50 ms, scan rate: 20 mV/s.

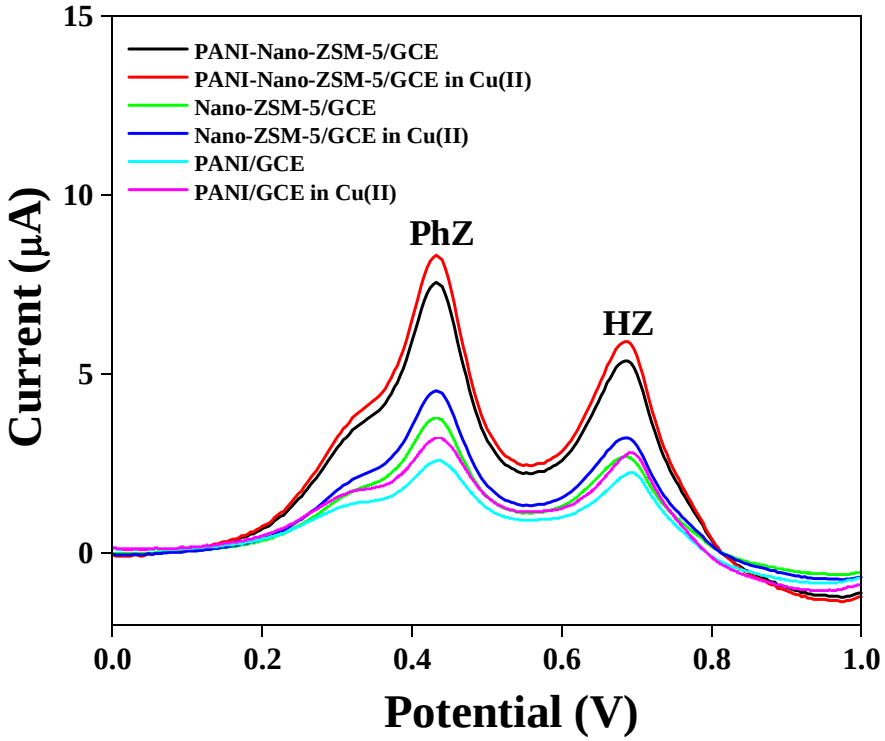

Figure S12. Comparison of DPV of binary mixture containing 5 μM each of PhZ and HZ at various modified electrodes {in the presence of 50 μM $CuCl_2$ in the electrochemical cell along with PhZ and HZ (PANI-Nano-ZSM-5/GCE in Cu(II), Nano-ZSM-5/GCE in Cu(II), PANI/GCE in Cu(II)) and in the absence of $CuCl_2$ (PANI-Nano-ZSM-5/GCE, Nano-ZSM-5/GCE, PANI/GCE)} in 0.1 M PBS (pH 8.5). DPV parameters were selected as: pulse amplitude: 50 mV, pulse width: 50 ms, scan rate: 20 mV/s.

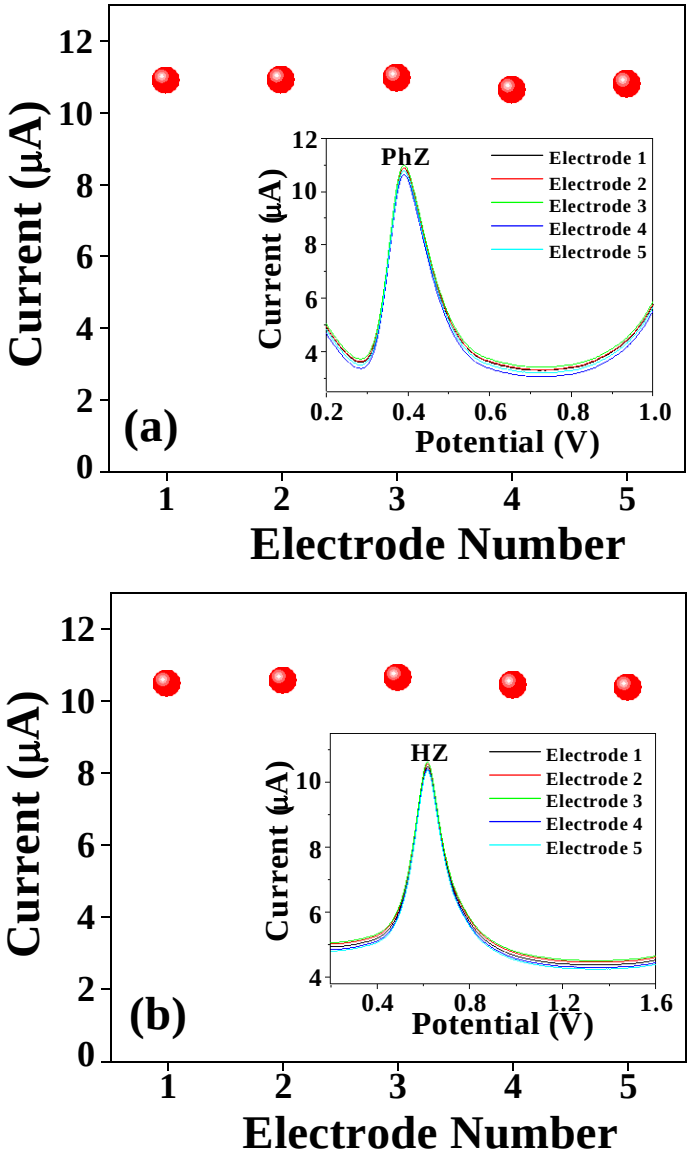

Figure S13. The current response at different freshly prepared Cu(5%)-PANI-Nano-ZSM-5/GCEs (n=5) in the presence of 1 μM each of (a) PhZ and (b) HZ. Inset shows corresponding DPV curves at 5 different Cu(5%)-PANI-Nano-ZSM-5/GCEs in the presence of 1 μM each of PhZ and HZ.

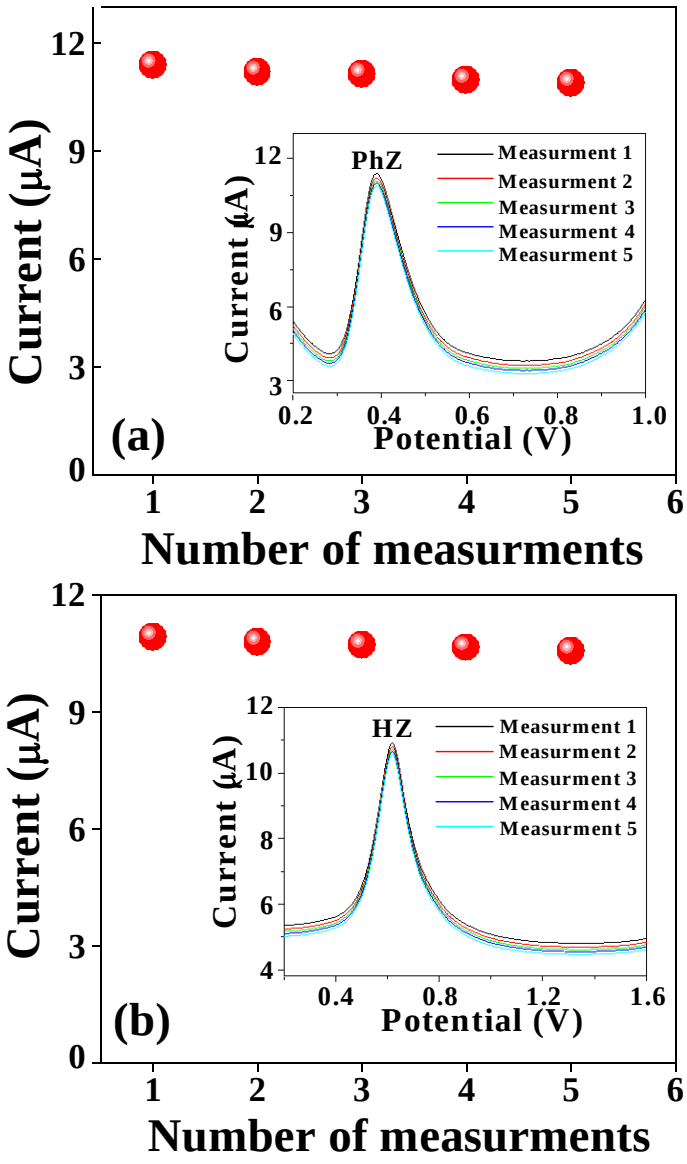

Figure S14. The current response at five different measurements (20 days time period at the interval of every 5 days) using same Cu(5%)-PANI-Nano-ZSM-5/GCE in the presence of 1 μM each of (a) PhZ and (b) HZ. Inset shows corresponding DPV curves at 5 different measurements using same Cu(5%)-PANI-Nano-ZSM-5/GCE in the presence of in the presence of 1 μM each of PhZ and HZ for 20 days time period at the interval of every 5 days.

Table S1. Comparison of Cu(5%)-PANI-Nano-ZSM-5/GCE with other electrodes reported in the literature for HZ and PhZ detection.

S.No.	Electrode material	Analyte	Linear range (M)	Detection limit (M)	Reference
1.	Co_3O_4 nanowires	HZ	20 µM – 700 µM	500 nM	[8]
2.	4-((2-hydroxy phenyl imino)methyl)benzene-1,2-diol-multi wall carbon nanotube	HZ	4 µM – 750.4 µM	1.1 µM	[9]
3.	Au/HDT/4α-Ni^{II}TAPc-AuNPs	HZ	10 µM – 100 µM	50 nM	[10]
4.	ZnO nanonails	HZ	0.1 µM – 1.2 µM	200 nM	[11]
5.	ZnO nanorod/SWCNT	HZ	0.5 µM – 50 µM	170 µM	[12]
6.	$Ni(OH)_2$–MnO_2	HZ	5 µM – 18 mM	120 nM	[13]
7.	Flower shape CuO	PhZ	5 µM – 10 mM	1.9 µM	[14]
8.	Ag-doped ZnO	PhZ	10^{-8} M – 10^{3} M	5 nM	[15]
9.	poly(o-anisidine)	PhZ	1.5 µM – 38 µM	900 µM	[16]
10.	(2,2′[1,2 butanediyl bis(nitriloethylidyne)]-bis-hydroquinone and TiO_2	PhZ HZ	2 µM – 1000 µM 75 µM – 1000 µM	0.75 µM 9 µM	[17]
11.	Cu(5%)-PANI-Nano-ZSM-5	PhZ HZ	4 nM – 800 µM 4 nM – 800 µM	1 nM 1 nM	This work

References

1. M. Sharp, M. Petersson and K. Edström, *J. Electroanal. Chem.*, 1979, **95**, 123.
2. Z. Galus, G. Reynolds and S. Marcinkiewicz, Fundamentals of electrochemical analysis, *Ellis Horwood Chichester*, 1976, **328**.
3. M. Baibarac, I. Baltog, S. Lefrant, J. Y. Mevellec and O. Chauvet, *Chem. Mater.*, 2003, **15**, 4149.
4. Y.-G. Wang, W. Wu, L. Cheng, P. He, C.-X. Wang and Y.-Y. Xia, *Adv. Mater.*, 2008, **20**, 2166.
5. M. U. Anu Prathap, R. Srivastava and B. Satpati, *Electrochim. Acta*, 2013, **114**, 285.
6. P. Ratnasamy, D. Srinivas and H. Knözinger, *Adv. Catal.*, 2004, **48**, 1.
7. D. Jung, C. Streb and M. Hartmann, *Int. J. Mol. Sci.*, 2010, **11**, 762.
8. J. Zhang, W. Gao, M. Dou, F. Wang, J. Liu, Z. Li and J. Ji, *Analyst*, 2015.
9. H. R. Zare, Z. Shekari, N. Nasirizadeh and A. A. Jafari, *Catal. Sci. Tech.*, 2012, **2**, 2492.
10. A. J. Jeevagan and S. A. John, *RSC Adv.*, 2013, **3**, 2256.
11. A. Umar, M. M. Rahman, S. H. Kim and Y.-B. Hahn, *Chem. Commun.*, 2008, 166.
12. K. NamáHan, C. AiáLi, M.-P. NgocáBui and G. HunáSeong, *Chem. Commun.*, 2011, **47**, 938.
13. M. U. Anu Prathap, V. Anuraj, B. Satpati and R. Srivastava, *J. Hazard. Mater.*, 2013, **262**, 766.
14. S. B. Khan, M. Faisal, M. M. Rahman, I. Abdel-Latif, A. A. Ismail, K. Akhtar, A. Al-Hajry, A. M. Asiri and K. A. Alamry, *New J. Chem.*, 2013, **37**, 1098.
15. A. A. Ibrahim, G. Dar, S. A. Zaidi, A. Umar, M. Abaker, H. Bouzid and S. Baskoutas, *Talanta*, 2012, **93**, 257.
16. R. Ojani, J.-B. Raoof and S. Zamani, *Appl. Surf. Sci.*, 2013, **271**, 98.
17. F. Gholamian, M. A. Sheikh-Mohseni and H. Naeimi, *Mat. Sci. Eng. C*, 2012, **32**, 2344.